International Journal of Control

ISSN: (Print) (Online) Journal homepage: https://www.tandfonline.com/loi/tcon20

Estimation and compensation of DC-Link voltage disturbances in a DC–DC converter for battery emulation

Alexander Wasserburger , Oliver König & Stefan Jakubek

To cite this article: Alexander Wasserburger , Oliver König & Stefan Jakubek (2020) Estimation and compensation of DC-Link voltage disturbances in a DC–DC converter for battery emulation, International Journal of Control, 93:4, 922-933, DOI: 10.1080/00207179.2019.1626994

To link to this article: https://doi.org/10.1080/00207179.2019.1626994

Published online: 13 Jun 2019.

INTERNATIONAL JOURNAL OF CONTROL
2020, VOL. 93, NO. 4, 922–933
https://doi.org/10.1080/00207179.2019.1626994

Taylor & Francis
Taylor & Francis Group

Estimation and compensation of DC-Link voltage disturbances in a DC–DC converter for battery emulation

Alexander Wasserburger[a], Oliver König[b] and Stefan Jakubek[c]

[a]Christian Doppler Laboratory for Innovative Control and Monitoring of Automotive Powertrain Systems, TU Wien, Vienna, Austria; [b]AVL List GmbH, Graz, Austria; [c]Division of Control and Process Automation, Institute of Mechanics and Mechatronics, TU Wien, Vienna, Austria

ABSTRACT

Battery emulation is essential for reliable testing of powertrains of electric and hybrid vehicles under repeatable conditions. For that purpose, a DC voltage controller provides fast reference tracking capabilities. Due to imperfect conversion of AC current to DC current, the DC voltage source of the battery emulator does not provide constant voltage but is subject to periodic fluctuations. This disturbance is propagated through the system to the battery emulator's output. In this paper, an observer-based compensation strategy is deployed. As the structure of the multiplicative perturbation is known, it is integrated into the battery emulator model yielding a state-affine system. An appropriate observer provides asymptotically correct estimates of the disturbance, which are then used to adequately manipulate the control variable without interfering with stability properties of the closed-loop system. Simulation and experimental results show the improvements achieved by the disturbance rejection.

ARTICLE HISTORY
Received 24 August 2017
Accepted 25 May 2019

KEYWORDS
Battery emulation; disturbance compensation; non-linear observer; hybrid powertrain testing; state-affine systems

1. Introduction

The electrification of automotive powertrains is a complex challenge that requires sophisticated electrical component test systems. Batteries are certainly among the most vital elements of powertrains for hybrid and electric vehicles. However, using real batteries in test beds is often not feasible for several reasons: (i) at early development stages, a battery might not be available, (ii) due to battery ageing, tests are not exactly reproducible, and (iii) preparing the physical batteries for specific operating conditions (like cold temperatures) is time-consuming and costly (König, Gregorčič, & Jakubek, 2013). To meet these challenges, battery emulators are deployed to replace batteries in test beds.

A battery emulator basically consists of a DC–DC step-down converter (buck converter), which is connected to a unit-under-test, a model of the physical battery and a voltage source. A schematic is depicted in Figure 1. The battery emulator is required to provide an output voltage v_2 matching the reference value v^*, which is provided by an appropriate battery model. This reference tracking has to achieve a high accuracy under all operating conditions independent of the unit-under-test. Since the system is supplied by an AC power source, a rectifier first has to convert the current to be used by the battery emulator. Periodic fluctuations in the voltage source supplying the emulator are generally a noteworthy problem in the control of battery emulators. In this paper, we show how to deal with these interferences by means of an exogenous disturbance model with a suitable observation and compensation structure. The considered perturbations stem from the inevitably imperfect conversion from AC current to DC current, which implies that the obtained DC-link voltage, denoted by V_0, is not constant, as explicitly assumed in König, Jakubek, and Prochart (2011), but rather oscillates around the target value. However, V_0 is crucial in the calculation of the duty cycles $d_a - d_c$ of the pulse width modulation. If the exact value of V_0 is not known, it is impossible to adequately control the half-bridges. Therefore, the disturbance acting on V_0 is propagated through the entire system and consequently, the battery emulator's output oscillates as well. This implies that the regulated voltage cannot follow the reference value with the demanded accuracy. The impact of this disturbance propagation is especially relevant at high voltage levels because the fluctuations in V_0 can only advance through the system, when the upper switches of the half-bridges are closed. Otherwise, there is no connection between the error-source and the emulator's output. When operating at high voltage levels, however, the duty cycle is close to 100%, which means that the half-bridges are closed most of the time during one sampling interval. Consequently, we observe even larger output fluctuations. This is of course very undesirable, since a battery emulator is in particular deployed to emulate extreme voltage trajectories. In order to ensure high performance in all operating ranges, the perturbations in the DC-link voltage have to be compensated.

The battery emulator used in this paper is controlled by a model predictive control (MPC) algorithm as described in König et al. (2011), König et al. (2013), König, Hametner, Prochart, and Jakubek (2013), König, Hametner, Jakubek, and Prochart (2015). In the literature also various other control strategies are described (see Alsmadi, Utkin, Haj-ahmed, & Xu, 2017; Ciezki & Ashton, 1998; Emadi, Khaligh, Rivetta, & Williamson, 2006; Rahimi & Emadi, 2009). Interestingly,

CONTACT Alexander Wasserburger alexander.wasserburger@tuwien.ac.at Christian Doppler Laboratory for Innovative Control and Monitoring of Automotive Powertrain Systems, TU Wien, Getreidemarkt 9/E325, 1060 Vienna, Austria

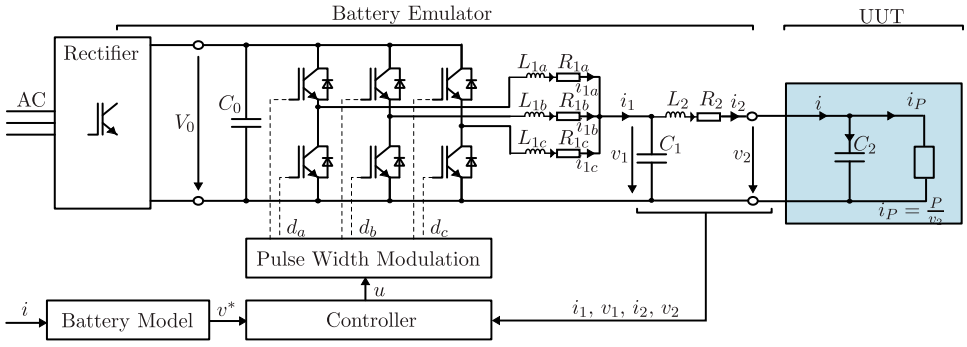

Figure 1. Schematic diagram of the battery emulator and unit-under-test.

none of these references consider the case, where the system's voltage source is not constant. It has to be kept in mind, though, that adding an observer-based compensation algorithm to an existing controller adds another feedback loop which potentially affects the closed-loop behaviour of the entire system (see Jakubek & Jörgl, 2000), possibly leading to instability. This is due to the fact that there is no controller-observer separation property for general non-linear systems (see Fuhrmann, Euler-Rolle, Killian, Reinwald, & Jakubek, 2017). So it is an additional requirement that the compensation scheme does not interfere with the pre-existing control architecture and its stability properties.

Disturbances or uncertainties are generally widespread and manifold in industrial applications. Consequently, disturbance rejection is of utmost importance in control system design (Gao, 2014; Guo & Wen-Hua, 2005; Li, Yang, Chen, & Chen, 2014). In the area of harmonic compensation in power distribution systems, passive and active power filters are common. For example, in Lascu, Asiminoaei, Boldea, and Blaabjerg (2007) and Lascu, Asiminoaei, Boldea, and Blaabjerg (2009), control strategies for active power filters are designed and analysed. The drawback of such filters is that their application involves physical devices like transistors that are added to the power grid. However, in this article, it is required that the existing battery emulator set-up remains unchanged and the disturbance compensation is a purely software-based solution. Therefore, disturbance-observer-based control (DOBC) is applied, which is another prominent approach for tackling the problem of disturbance rejection. DOBC-strategies at first emerged in the 1980s and since then have been implemented in various areas, such as flight control, mechanical engineering and chemical processes (see Chen, Li, Yang, & Li, 2013; de Jesús Rubio, Meléndez, & Figueroa, 2014; Yang, Li, Sun, & Guo, 2013). There are numerous different variations of DOBC. A broad survey of existing techniques is outlined in Chen, Yang, Guo, and Li (2016). The general idea, that all the proposed methods have in common, is to estimate the perturbations by means of an adequate observer and to use that estimation in order to compensate the disturbance.

When it comes to the selection of a suitable observer, vast literature is accessible. For linear systems, the Luenberger observer (Luenberger, 1964) and the Kalman filter (Kalman, 1960) are among the most established techniques. In the non-linear case, generalisations of the above-mentioned methods exist, as well as other types of observers, such as high-gain observers (Adamy, 2009) or sliding mode observers (Floquet, Barbot, Perruquetti, & Djemai, 2004).

In this paper, however, we can make good use of observers for state-affine systems as described in Hammouri and de Leon Morales (1990), Bornard, Couenne, and Celle (1989), Besancon, León-Morales, and Huerta-Guevara (2006), Klein and Olbrot (1986), Bara, Daafouz, Kratz, and Ragot (2001). More precisely, we are interested in systems of the form

$$\begin{aligned} \dot{\boldsymbol{x}} &= \boldsymbol{A}(u)\boldsymbol{x} + \boldsymbol{B}u \\ \boldsymbol{y} &= \boldsymbol{C}\boldsymbol{x}, \end{aligned} \tag{1}$$

where $\boldsymbol{x} \in \mathbb{R}^n$ is the vector of states, $u \in \mathbb{R}$ is the input determined by the controller, $\boldsymbol{A}(u) \in \mathbb{R}^{n\times n}$ is the system matrix that depends on u, $\boldsymbol{B} \in \mathbb{R}^{n\times 1}$ is the input matrix, $\boldsymbol{y} \in \mathbb{R}^m$ is the vector of measurable outputs and $\boldsymbol{C} \in \mathbb{R}^{m\times n}$ is the output matrix. We obtain such a state-affine system (1) by augmenting the linear battery emulator model with an exogenous disturbance model, where the unknown perturbation acts multiplicatively on the input-variable u. The exogenous model is based on a-priori expert knowledge and is defined as a harmonic oscillation with a fixed and known frequency. In Yang, Cui, Li, and Zolotas (2018) and Yang, Wu, Hu, and Li (2018), active disturbance rejection for DC–DC converters using generalised proportional integral observers is demonstrated. While this approach satisfyingly rejects various types of disturbances and uncertainties, periodic oscillations in the voltage supply are only mitigated to some extent but not completely compensated. There are several works dealing specifically with the rejection of periodic disturbances using internal model control or adaptive feedforward cancellation (Bodson, 2001; Francis & Wonham, 1976). References (Bodson & Douglas, 1997; Bodson, Sacks, & Khosla, 1994; Marino, Santosuosso, & Tomei, 2003) deal with the rejection of periodic disturbances of unknown frequencies making use of adaptive feedforward schemes. However, these references are exclusively concerned with additive disturbances. The battery emulator we are dealing with in this paper is affected by multiplicative disturbances, though. Moreover, our approach leaves the existing controller structure untouched and can simply be added to a running system.

This paper is structured as follows: In Section 2, the models of the battery emulator and the disturbance are stated. In Section 3, these two models are combined and the disturbance observer is introduced. Stability proofs for the observer and the

closed loop system with compensation are given. Moreover a simplified linear version of the observer is introduced at the end of this section. Simulation and experimental results are presented in Section 4.

2. System description

2.1 Working principles of the battery emulator

The parallel battery emulation half bridges are configured as an interleaving DC–DC converter. The duty cycle is applied equally to all half bridges with an additional offset for current balancing between the half bridges. See König et al. (2013) for a description of how to combine all duty cycles to one control signal. See Correa, König, and Greul (2016) for an approach to implement the interleaving.

The involved rectifier is configured as an active frontend rectifier (AFE) with IGBT half bridges and voltage oriented control. The test system also uses IGBTs as power switches. Of course, the non-ideal characteristics of the power switches, like interlock dead times, have an effect on the system's performance. However, describing and compensating these effects is not the intended scope of this paper.

In this article, the examined disturbance stems from the AFE. Theoretically, it is possible to achieve a constant power flow with a 3-phase AFE such that the DC-link voltage contains no grid frequency harmonics. However, in a practical implementation, there are several reasons for residual DC-link oscillations. The main reasons are: (i) measurement errors of grid current sensors: an offset error of one sensor causes a 50 Hz ripple, a gain error of one sensor results in 100 Hz ripple for 50 Hz AC. (ii) the DC-link voltage sensor, which is required as a feedback signal to the rectifier controller, is disturbed through auxiliary power supply, inductive and capacitive coupling. The disturbances are therefore mainly harmonics of the grid frequency including the base frequency of 50 Hz. The disturbances in this work are consequently modelled as sinusoids with known frequencies. Even if the disturbance is not an ideal sinusoid, it is still possible to compensate the disturbance to a large extent by assuming it is purely sinusoidal. Any non-sinusoidal but periodic disturbance can be seen as a superposition of individual harmonic disturbances. In a first step, the proposed observer is set to the dominant harmonic (in most cases including skewed sinusoids, this will be the base frequency). In a second step, it is possible to use multiple instances of the observer to compensate the remaining harmonics. A picture of the battery emulator is shown in Figure 2.

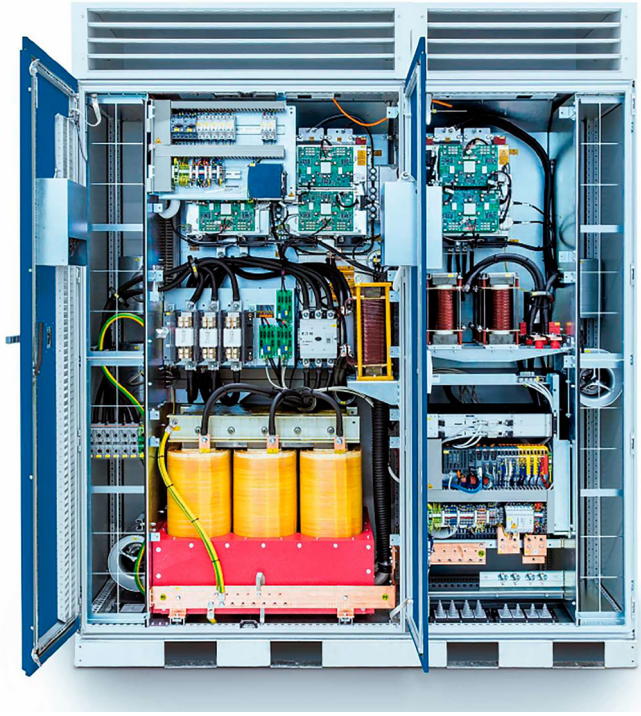

Figure 2. The battery emulator used in this article. The left part of the cabinet contains the AC grid input, isolation transformer and the active frontend (AFE). The right part contains the DC–DC converter.

2.2 Battery emulator model

The electric circuit of the battery emulator is depicted in Figure 1. The controller determines the input voltage variable u according to the state measurements and the reference voltage v^*. The control signal u, however, is transformed into three duty cycles d_a, d_b and d_c which control the half bridges via pulse width modulation. The output stage is assumed to have equal inductances $L_{1a} = L_{1b} = L_{1c}$ and phase inductor resistances $R_{1a} = R_{1b} = R_{1c}$. Hence, the three inductors can be considered to be connected in parallel such that they are replaced by one inductance $L_1 = \frac{1}{3}L_{1a}$ with $R_1 = \frac{1}{3}R_{1a}$ and a common duty cycle $d = d_a = d_b = d_c$. The duty cycle is therefore given by $d = \frac{u}{V_0}$, where V_0 is the nominal constant DC-link voltage assumed for the pulse width modulation and u is the manipulated variable. As a matter of fact, because of the defective conversion of AC current to DC current performed by the rectifier, this assumption does not hold, leading to a corrupted duty cycle. The filter dynamics are described by a state space model based on the physical properties of the circuit elements. C_1 and C_2 denote filter capacitances. The cable connecting the battery emulator and the unit-under-test is modelled as a series connection of an inductance L_2 and a resistance R_2. The state vector is defined as $\boldsymbol{x}_m = [i_1, v_1, i_2, v_2]^T$, where i_j and v_j, $j = 1, 2$ represent currents and voltages, respectively. The load current is denoted by i. Kirchhoff's circuit laws then yield the following state-space model with input $u \in \mathbb{R}$ and output $\boldsymbol{y}_m \in \mathbb{R}^4$:

$$\begin{aligned}\dot{\boldsymbol{x}}_m = &\underbrace{\begin{pmatrix} -\frac{R_1}{L_1} & -\frac{1}{L_1} & 0 & 0 \\ \frac{1}{C_1} & 0 & -\frac{1}{C_1} & 0 \\ 0 & \frac{1}{L_2} & -\frac{R_2}{L_2} & -\frac{1}{L_2} \\ 0 & 0 & \frac{1}{C_2} & 0 \end{pmatrix}}_{\boldsymbol{A}_m} \boldsymbol{x}_m \\ &+ \underbrace{\begin{pmatrix} \frac{1}{L_1} \\ 0 \\ 0 \\ 0 \end{pmatrix}}_{\boldsymbol{B}_m} u + \underbrace{\begin{pmatrix} 0 \\ 0 \\ 0 \\ -\frac{1}{C_2} \end{pmatrix}}_{\boldsymbol{E}_m} i \\ \boldsymbol{y}_m = &\boldsymbol{x}_m \end{aligned} \tag{2}$$

Table 1. Baseline parameters for the battery emulator.

R_1	R_2	L_1	L_2	C_1	C_2	V_0
0.08 Ω	0.05 Ω	75 µH	12.5 µH	1575 µF	2300 µF	820 V

Since all states can be measured, the output vector $\boldsymbol{y}_m$ equals the state vector $\boldsymbol{x}_m$. The controlled variable is the output voltage v_2. A baseline parametrisation is presented in Table 1.

2.3 Disturbance of the DC-Link voltage

As mentioned in Section 1, the real value of V_0 (denoted by V_0^*) is not constant but subject to periodic, sinusoidal disturbances, which are not considered by the controller:

$$V_0^*(t) = V_0 + \zeta_1 \sin(2\pi f_1 t + \varphi_1) + \zeta_2 \sin(2\pi f_2 t + \varphi_2) + \dots, \tag{3}$$

where the amplitudes ζ_j and phases φ_j are unknown and the frequencies f_j, $j = 1, \dots$ are known to be multiples of 50 Hz. The control infrastructure calculates the duty cycle d with the constant value V_0 when in reality V_0^* should be used. Therefore, the duty cycle does not precisely reflect the demanded voltage u and thus the voltage applied to the system does not equal the value demanded by the controller. In terms of the model formulation, because of the relation $u = V_0 d$, the corrupted DC-link voltage V_0^* yields a disturbed input signal u^*:

$$u^* = V_0^* d = u + \frac{u\zeta_1 \sin(2\pi f_1 t + \varphi_1)}{V_0} + \dots \tag{4}$$

Note that the disturbance $\zeta_j \sin(2\pi f_j t + \varphi_j)$ is not simply added to u but rather acts multiplicatively on $\frac{u}{V_0}$.

As a result of the disturbed input u^*, the controlled voltage v_2 oscillates around the desired setpoint. This is especially relevant at high voltage levels, because the disturbance is amplified by u as it can be seen in (4).

3. Observation and compensation

3.1 System augmentation

With the structure of the disturbance being known, we can incorporate its effect in the model. Furthermore, for now, we assume that the disturbance comprises only one frequency f and the value of f is known. The differential equation of a harmonic oscillation with frequency f, as described in (3), is given by

$$\ddot{z} = -\omega^2 z \tag{5}$$

with $\omega = 2\pi f$. Transforming (5) into a first-order differential equation system with a state vector $\boldsymbol{x}_z = [a_1, a_2]^T$, the disturbance $z = a_1$ can now be written as

$$\begin{aligned} \dot{\boldsymbol{x}}_z &= \underbrace{\begin{pmatrix} 0 & 1 \\ -\omega^2 & 0 \end{pmatrix}}_{\boldsymbol{A}_z} \boldsymbol{x}_z \\ z &= \underbrace{[1 \;\; 0]}_{\boldsymbol{C}_z} \boldsymbol{x}_z. \end{aligned} \tag{6}$$

Expressing the disturbance term in (4) by means of (6), we obtain

$$u^* = u + \frac{\boldsymbol{C}_z \boldsymbol{x}_z u}{V_0}. \tag{7}$$

Combining the emulator model (2), the disturbance model (6), and the disturbed control input (7), yields the following augmented model with a new state vector $\boldsymbol{x} = [i_1, v_1, i_2, v_2, a_1, a_2]^T$:

$$\begin{aligned} \underbrace{\begin{pmatrix} \dot{\boldsymbol{x}}_m \\ \dot{\boldsymbol{x}}_z \end{pmatrix}}_{\dot{\boldsymbol{x}}} &= \underbrace{\left(\begin{array}{c|c} \boldsymbol{A}_m & \frac{1}{V_0}\boldsymbol{B}_m \boldsymbol{C}_z u \\ \hline \boldsymbol{0}_{2,4} & \boldsymbol{A}_z \end{array}\right)}_{\boldsymbol{A}(u)} \underbrace{\begin{pmatrix} \boldsymbol{x}_m \\ \boldsymbol{x}_z \end{pmatrix}}_{\boldsymbol{x}} + \underbrace{\begin{pmatrix} \boldsymbol{B}_m \\ \boldsymbol{0}_{2,1} \end{pmatrix}}_{\boldsymbol{B}} u + \underbrace{\begin{pmatrix} \boldsymbol{E}_m \\ \boldsymbol{0}_{2,1} \end{pmatrix}}_{\boldsymbol{E}} i \\ \boldsymbol{y} &= \underbrace{\begin{pmatrix} 1 & 0 & 0 & 0 & 0 & 0 \\ 0 & 1 & 0 & 0 & 0 & 0 \\ 0 & 0 & 1 & 0 & 0 & 0 \\ 0 & 0 & 0 & 1 & 0 & 0 \end{pmatrix}}_{\boldsymbol{C}} \boldsymbol{x} = \begin{pmatrix} i_1 \\ v_1 \\ i_2 \\ v_2 \end{pmatrix}. \end{aligned} \tag{8}$$

$\boldsymbol{0}_{m,n}$ stands for a $m \times n$ zero-matrix. Note that the disturbance acting on u is now incorporated in the system matrix $\boldsymbol{A}(u)$ resulting in a state-affine system. This augmented model can now be used to formulate an observer that estimates the unknown disturbance-variable $z = a_1$ for a fixed frequency f. If several frequencies are to be observed simultaneously, the model can be extended accordingly (two additional equations for each frequency). Also constant offsets can be included by setting $\omega = 0$. As the total disturbance of the DC-link voltage is modelled as a sum of independent sine waves with different amplitudes, frequencies and phase shifts (see (3)), the proposed method cannot only measure sinusoidal disturbances but all kinds of signals that can be approximated by means of a Fourier approximation as long as the signal's harmonics are somewhat similar to the ones defined in the augmented system (8). Moreover, if the most important harmonics of the disturbance signal can be estimated from measurements, the system can be augmented with exactly these frequencies. As a result, various shapes of disturbances can be estimated and the method is not limited to pure sinusoidal disturbance. Without loss of generality, in this article we focus exclusively on the case of one sinusoidal disturbance to be estimated.

3.2 Observer design

An observer for the state-affine system (8), as proposed in Bornard et al. (1989), is given by

$$\begin{aligned} \dot{\hat{\boldsymbol{x}}} &= \boldsymbol{A}(u)\hat{\boldsymbol{x}} - \boldsymbol{S}^{-1}\boldsymbol{C}^T(\boldsymbol{C}\hat{\boldsymbol{x}} - \boldsymbol{C}\boldsymbol{x}) + \boldsymbol{B}u + \boldsymbol{E}i \\ \dot{\boldsymbol{S}} &= -\psi \boldsymbol{S} - \boldsymbol{A}(u)^T\boldsymbol{S} - \boldsymbol{S}\boldsymbol{A}(u) + \boldsymbol{C}^T\boldsymbol{C} \\ \boldsymbol{S}(0) &= \boldsymbol{S}_0 \succ 0, \psi \in \mathbb{R}_+. \end{aligned} \tag{9}$$

$\boldsymbol{S}(t)$ is a time-dependant matrix with the same dimension as $\boldsymbol{A}(u)$. For a positive definite initial value $\boldsymbol{S}_0$, the matrix $\boldsymbol{S}(t)$ is guaranteed to be positive definite for all $t > 0$. Therefore, the inverse matrix $\boldsymbol{S}(t)^{-1}$ exists for all t and the observer is well-defined. The positive, real parameter ψ is a tuning parameter which basically defines the speed of convergence of the observation error. For so-called ψ-strictly persistent inputs the

exponential convergence of the observer can be shown using Lyapunov theory with time-varying Lyapunov functions (see Khalil, 2002). The input u is said to be ψ-strictly persistent if:

$$\begin{aligned}&\exists \gamma, \bar{t} > 0 : \forall t \geq \bar{t} : \\ &\int_0^t \mathrm{e}^{-\psi(t-\sigma)} \boldsymbol{\Phi}_u(\sigma, t)^T \boldsymbol{C}^T \boldsymbol{C} \boldsymbol{\Phi}_u(\sigma, t)\, d\sigma \succcurlyeq \gamma \boldsymbol{I},\end{aligned} \tag{10}$$

where the state-transition matrix $\boldsymbol{\Phi}_u(s, t_0)$ is the unique solution of

$$\begin{aligned}\frac{\mathrm{d}}{\mathrm{d}s} \boldsymbol{\Phi}_u(s, t_0) &= \boldsymbol{A}(u) \boldsymbol{\Phi}_u(s, t_0) \\ \boldsymbol{\Phi}_u(t_0, t_0) &= \boldsymbol{I}.\end{aligned} \tag{11}$$

For more details and a proof of convergence, we refer to Hammouri and de Leon Morales (1990) and Bornard et al. (1989).

The observer (9) has two major drawbacks: Firstly, solving the matrix differential equation for $\boldsymbol{S}$ significantly increases the computational load. Secondly, analytically verifying condition (10) is challenging. Therefore, we propose another observer, inspired by (9):

$$\dot{\hat{\boldsymbol{x}}} = \boldsymbol{A}(u)\hat{\boldsymbol{x}} - \boldsymbol{S}^{-1}\boldsymbol{C}^T(\boldsymbol{C}\hat{\boldsymbol{x}} - \boldsymbol{C}\boldsymbol{x}) + \boldsymbol{B}u + \boldsymbol{E}i, \tag{12}$$

where $\boldsymbol{S}$ is now a constant positive definite matrix, that has to be determined in such a way that the observation error $\boldsymbol{\varepsilon} := \boldsymbol{x} - \hat{\boldsymbol{x}}$ goes to zero exponentially:

$$\exists k, \alpha > 0 : \forall t > 0 : ||\boldsymbol{\varepsilon}(t)||_2^2 \leq k\mathrm{e}^{-\alpha t}. \tag{13}$$

We obtain conditions for a suitable matrix $\boldsymbol{S}$ using Lyapunov theory: Differentiating $\boldsymbol{\varepsilon}$ with respect to time yields

$$\dot{\boldsymbol{\varepsilon}} = \dot{\boldsymbol{x}} - \dot{\hat{\boldsymbol{x}}} = \left(\boldsymbol{A}(u) - \boldsymbol{S}^{-1}\boldsymbol{C}^T\boldsymbol{C}\right)\boldsymbol{\varepsilon}. \tag{14}$$

Obviously, $\boldsymbol{\varepsilon} = 0$ is an equilibrium of system (14). If we can find a Lyapunov function $V(\boldsymbol{\varepsilon})$ such that

$$\dot{V}(\boldsymbol{\varepsilon}) \leq -\alpha V(\boldsymbol{\varepsilon}) \tag{15}$$

with $\alpha > 0$, then the steady state $\boldsymbol{\varepsilon} = 0$ is exponentially stable (see Khalil, 2002).

Define $V(\boldsymbol{\varepsilon}) := \boldsymbol{\varepsilon}^T\boldsymbol{S}\boldsymbol{\varepsilon}$. Differentiating V with respect to time yields:

$$\begin{aligned}\dot{V}(\boldsymbol{\varepsilon}) &= \dot{\boldsymbol{\varepsilon}}^T\boldsymbol{S}\boldsymbol{\varepsilon} + \boldsymbol{\varepsilon}^T\boldsymbol{S}\dot{\boldsymbol{\varepsilon}} \\ &= \boldsymbol{\varepsilon}^T\left(\boldsymbol{A}(u) - \boldsymbol{S}^{-1}\boldsymbol{C}^T\boldsymbol{C}\right)^T\boldsymbol{S}\boldsymbol{\varepsilon} \\ &\quad + \boldsymbol{\varepsilon}^T\boldsymbol{S}\left(\boldsymbol{A}(u) - \boldsymbol{S}^{-1}\boldsymbol{C}^T\boldsymbol{C}\right)\boldsymbol{\varepsilon} \\ &= \boldsymbol{\varepsilon}^T\left(\boldsymbol{A}(u)^T\boldsymbol{S} + \boldsymbol{S}\boldsymbol{A}(u) - 2\boldsymbol{C}^T\boldsymbol{C}\right)\boldsymbol{\varepsilon}\end{aligned} \tag{16}$$

Consequently, according to (15), a sufficient condition for exponential stability is

$$\underbrace{\boldsymbol{A}(u)^T\boldsymbol{S} + \boldsymbol{S}\boldsymbol{A}(u) - 2\boldsymbol{C}^T\boldsymbol{C} + \alpha\boldsymbol{S}}_{=:\boldsymbol{W}(u)} \preccurlyeq 0. \tag{17}$$

We have to ask whether this condition can be fulfilled for all u. In the case $u = 0$, we can derive from (8) that $\boldsymbol{x}_m$ and $\boldsymbol{x}_z$ are completely independent from each other, so there is no way to reconstruct $\boldsymbol{x}_z$ from the measurements of $\boldsymbol{x}_m$. However, for small, positive values of u the effects of the disturbance are generally insignificant as seen in (7). Therefore, for $0 \leq u < u_{\min}$ there is no need for observation and compensation. Apart from the condition $u \geq u_{\min}$, we also need to restrict the space of admissible inputs u from above:

Theorem 3.1: *Let $\boldsymbol{S}$ be an arbitrary positive definite matrix of appropriate size. There exists a $\bar{u} > 0$ with $\boldsymbol{W}(\bar{u}) \not\preccurlyeq 0$.*

Proof: Using the decomposition

$$\begin{aligned}\underbrace{\left(\begin{array}{c|c}\boldsymbol{A}_m & \frac{1}{V_0}\boldsymbol{B}_m\boldsymbol{C}_z u \\ \hline \boldsymbol{0}_{2,4} & \boldsymbol{A}_z\end{array}\right)}_{\boldsymbol{A}(u)} &= \underbrace{\left(\begin{array}{c|c}\boldsymbol{A}_m & \boldsymbol{0}_{4,2} \\ \hline \boldsymbol{0}_{2,4} & \boldsymbol{A}_z\end{array}\right)}_{\boldsymbol{A}_1} \\ &\quad + \underbrace{\left(\begin{array}{c|c}\boldsymbol{0}_{4,4} & \frac{1}{V_0}\boldsymbol{B}_m\boldsymbol{C}_z \\ \hline \boldsymbol{0}_{2,4} & \boldsymbol{0}_{2,2}\end{array}\right)}_{\boldsymbol{A}_2} u\end{aligned} \tag{18}$$

the quadratic form $\boldsymbol{x}^T\boldsymbol{W}(u)\boldsymbol{x}$ can be written as

$$\begin{aligned}\boldsymbol{x}^T\boldsymbol{W}(u)\boldsymbol{x} &= \boldsymbol{x}^T\left(\boldsymbol{A}_1^T\boldsymbol{S} + \boldsymbol{S}\boldsymbol{A}_1\right)\boldsymbol{x} + \boldsymbol{x}^T\underbrace{\left(\boldsymbol{A}_2^T\boldsymbol{S} + \boldsymbol{S}\boldsymbol{A}_2\right)}_{\boldsymbol{W}_\Delta}\boldsymbol{x}u \\ &\quad - 2\boldsymbol{x}^T\boldsymbol{C}^T\boldsymbol{C}\boldsymbol{x} + \alpha\boldsymbol{x}^T\boldsymbol{S}\boldsymbol{x}\end{aligned} \tag{19}$$

With $\boldsymbol{S} = (s_{i,j})_{i=1\ldots6;j=1\ldots6}$ and because of the simple structure of $\boldsymbol{A}_2$, the matrix $\boldsymbol{W}_\Delta$ has the following form:

$$\boldsymbol{W}_\Delta = \frac{1}{V_0 L_1}\underbrace{\begin{pmatrix}0 & 0 & 0 & 0 & s_{1,1} & 0 \\ 0 & 0 & 0 & 0 & s_{2,1} & 0 \\ 0 & 0 & 0 & 0 & s_{3,1} & 0 \\ 0 & 0 & 0 & 0 & s_{4,1} & 0 \\ s_{1,1} & s_{2,1} & s_{3,1} & s_{4,1} & 2s_{5,1} & s_{6,1} \\ 0 & 0 & 0 & 0 & s_{6,1} & 0\end{pmatrix}}_{\widetilde{\boldsymbol{W}}_\Delta}. \tag{20}$$

The matrix $\widetilde{\boldsymbol{W}}_\Delta$ has the eigenvalues $\lambda_1 = 0$ (with algebraic multiplicity 4) and $\lambda_{2,3} = s_{5,1} \pm \sqrt{s_{1,1}^2 + s_{2,1}^2 + s_{3,1}^2 + s_{4,1}^2 + s_{5,1}^2 + s_{6,1}^2}$. Since $\boldsymbol{S}$ is assumed to be positive definite, $s_{1,1}$ has to be greater than zero, according to Sylvester's criterion. Therefore, the square root is always larger than the absolute value of $s_{5,1}$. This implies that, independent of $\boldsymbol{S}$, there is always a positive eigenvalue of $\widetilde{\boldsymbol{W}}_\Delta$, denoted by λ_+, with a corresponding eigenvector $\boldsymbol{v}_+$. Setting $\boldsymbol{x} = \boldsymbol{v}_+$ in (19) and using the fact that $\boldsymbol{v}_+$ is an eigenvector, we obtain

$$\begin{aligned}\boldsymbol{v}_+^T\boldsymbol{W}(u)\boldsymbol{v}_+ &= \boldsymbol{v}_+^T\left(\boldsymbol{A}_1^T\boldsymbol{S} + \boldsymbol{S}\boldsymbol{A}_1\right)\boldsymbol{v}_+ + \underbrace{\frac{1}{V_0 L_1}||\boldsymbol{v}_+||_2^2\lambda_+}_{>0}u \\ &\quad - 2\boldsymbol{v}_+^T\boldsymbol{C}^T\boldsymbol{C}\boldsymbol{v}_+ + \alpha\boldsymbol{v}_+^T\boldsymbol{S}\boldsymbol{v}_+.\end{aligned} \tag{21}$$

The second term is positive and multiplied by u. All other terms are independent of u. This means that there is a $\bar{u}$ such

that the sum is dominated by the term containing $\bar{u}$, so that $\boldsymbol{v}_+^T \boldsymbol{W}(\bar{u})\boldsymbol{v}_+ > 0$, which means that $\boldsymbol{W}(\bar{u})$ is not negative semi-definite. ■

The above theorem shows that no matter how we choose $\boldsymbol{S}$, we cannot obtain stability for arbitrarily large inputs u. For every $\boldsymbol{S}$, there is an upper limit for u, above which the derivative of the Lyapunov function is not guaranteed to be negative. This is the consequence of abandoning the differential equation for $\boldsymbol{S}$. However, this fact is not necessarily an issue, since arbitrarily large voltages are not possible anyway and we just need to cover the operating range of the battery emulator. The highest voltage the battery emulator can deliver, is defined by the nominal DC-link voltage V_0, which is given by 820 V (see Table 1). With $u_{\max} = V_0 = 820$ and an appropriately chosen $u_{\min} > 0$ ($u_{\min}$ will be defined later), we now want to determine a positive definite matrix $\boldsymbol{S}$, so that

$$\boldsymbol{W}(u) \preccurlyeq 0, \forall u \in [u_{\min}, u_{\max}]. \tag{22}$$

The following theorem shows that it suffices to consider the negative semi-definiteness of $\boldsymbol{W}(u_{\min})$ and $\boldsymbol{W}(u_{\max})$:

Theorem 3.2: *Let $\boldsymbol{S}$ be an arbitrary matrix of appropriate size. If $\boldsymbol{W}(u) \preccurlyeq 0$ (see (17)) for $u = u_{\min}$ and $u = u_{\max}$, then $\boldsymbol{W}(u) \preccurlyeq 0, \forall u \in [u_{\min}, u_{\max}]$.*

Proof: Using (19), the quadratic form $\boldsymbol{x}^T\boldsymbol{W}(u)\boldsymbol{x}$ can also be written as

$$\begin{aligned}\boldsymbol{x}^T\boldsymbol{W}(u)\boldsymbol{x} = \boldsymbol{x}^T\left(\boldsymbol{A}_1^T\boldsymbol{S} + \boldsymbol{S}\boldsymbol{A}_1 - 2\boldsymbol{C}^T\boldsymbol{C} + \alpha\boldsymbol{S}\right)\boldsymbol{x} \\ + \boldsymbol{x}^T\boldsymbol{W}_\Delta\boldsymbol{x}u\end{aligned} \tag{23}$$

Assume there exists a $\bar{u}$ with $u_{\min} < \bar{u} < u_{\max}$ and $\boldsymbol{W}(\bar{u}) \not\preccurlyeq 0$. This implies that there exists a vector $\boldsymbol{x}$ with

$$\boldsymbol{x}^T\left(\boldsymbol{A}_1^T\boldsymbol{S} + \boldsymbol{S}\boldsymbol{A}_1 - 2\boldsymbol{C}^T\boldsymbol{C} + \alpha\boldsymbol{S}\right)\boldsymbol{x} + \boldsymbol{x}^T\boldsymbol{W}_\Delta\boldsymbol{x}\bar{u} > 0. \tag{24}$$

But, because of the negative semi-definiteness of $\boldsymbol{W}(u_{\min})$ and $\boldsymbol{W}(u_{\max})$, we also have

$$\boldsymbol{x}^T\left(\boldsymbol{A}_1^T\boldsymbol{S} + \boldsymbol{S}\boldsymbol{A}_1 - 2\boldsymbol{C}^T\boldsymbol{C} + \alpha\boldsymbol{S}\right)\boldsymbol{x} + \boldsymbol{x}^T\boldsymbol{W}_\Delta\boldsymbol{x}u_{\min} \le 0 \tag{25}$$

$$\boldsymbol{x}^T\left(\boldsymbol{A}_1^T\boldsymbol{S} + \boldsymbol{S}\boldsymbol{A}_1 - 2\boldsymbol{C}^T\boldsymbol{C} + \alpha\boldsymbol{S}\right)\boldsymbol{x} + \boldsymbol{x}^T\boldsymbol{W}_\Delta\boldsymbol{x}u_{\max} \le 0 \tag{26}$$

Since, for a fixed $\boldsymbol{x}$, (23) is a linear function in u, the inequalities (24)–(26) cannot be true at the same time. Therefore, a $\bar{u}$ with the above properties does not exist. ■

Thus, solving the following linear matrix inequality (LMI) guarantees a stable observer: Find a matrix $\boldsymbol{S}$ such that

$$\boldsymbol{W}(u_{\min}) \preccurlyeq 0 \tag{27}$$

$$\boldsymbol{W}(u_{\max}) \preccurlyeq 0 \tag{28}$$

$$\boldsymbol{S} \succ 0. \tag{29}$$

Additionally, the value of $u_{\min}$ can now be defined as

$$u_{\min} := \min\left\{u > 0 : \exists \boldsymbol{S} \succ 0 : \boldsymbol{W}(u) \preccurlyeq 0 \wedge \boldsymbol{W}(u_{\max}) \preccurlyeq 0\right\}. \tag{30}$$

Before solving system (27)–(29), the value of the parameter α, which defines the speed of convergence of the observer, has to be selected. A larger value implies faster convergence but makes solving the LMI-system harder. Setting $\alpha = 1$ and using the parameters from Table 1, we find a feasible solution $\boldsymbol{S}$ of system (27)–(29). The minimal voltage as defined in (30) turns out to be $u_{\min} = 0.49$. With the obtained matrix $\boldsymbol{S}$, the observation error $\boldsymbol{\varepsilon}$ converges to zero exponentially as long as the input u lies between 0.49 and 820. For $u < 0.49$, the propagated error is negligible and therefore the observation is irrelevant and can be switched off.

3.3 Compensation of the disturbance

In order to reject the disturbance, a suitable compensation signal has to be generated from the estimated disturbance $\hat{z} = \tilde{\boldsymbol{C}}\hat{\boldsymbol{x}}$ with $\tilde{\boldsymbol{C}} = [0\,0\,0\,0\,1\,0]$. The necessary fault compensation, denoted by c, is generated by

$$c = \frac{u\hat{z}}{V_0 + \hat{z}}. \tag{31}$$

The compensated signal u_{comp} is then defined as

$$u_{comp} = u - c, \tag{32}$$

where u is the original control signal determined by the controller. The choice of c ensures that the oscillations in V_0 are asymptotically compensated and the control signal u that was determined by the controller is effectively applied to the plant (i.e. $u = u^*$, see (7)), as we have $\hat{z} \to z$ asymptotically:

$$\begin{aligned}u^* &= u_{comp} + \frac{u_{comp}z}{V_0} = \frac{u-c}{V_0}(V_0 + z) = \\ &= \frac{u - \frac{u\hat{z}}{V_0+\hat{z}}}{V_0}(V_0 + z) = \frac{V_0 + z}{V_0 + \hat{z}}u \to u\end{aligned} \tag{33}$$

An overview of the method is given in Figure 3. The disturbed signal u^* enters the plant and the plant dynamics $\dot{\boldsymbol{x}}_m = \boldsymbol{A}_m\boldsymbol{x}_m + \boldsymbol{B}_m u^* + \boldsymbol{E}_m i$ lead to the measurable state vector $\boldsymbol{x}_m = [i_1, v_1, i_2, v_2]^T$. This state vector is fed back to the controller and to the disturbance observer. The observer has access to the augmented model (8) and to the compensated signal u_{comp}, which would enter the plant if there was no disturbance. The observer now basically compares the real plant output $\boldsymbol{x}_m = \boldsymbol{C}\boldsymbol{x}$ to the output $\boldsymbol{C}\hat{\boldsymbol{x}}$, which is affected by the estimated disturbance. The discrepancy $\boldsymbol{C}\hat{\boldsymbol{x}} - \boldsymbol{C}\boldsymbol{x}$ is used to adjust the current estimate of the disturbance following the observer equation $\dot{\hat{\boldsymbol{x}}} = \boldsymbol{A}(u_{comp})\hat{\boldsymbol{x}} - \boldsymbol{S}^{-1}\boldsymbol{C}^T(\boldsymbol{C}\hat{\boldsymbol{x}} - \boldsymbol{C}\boldsymbol{x}) + \boldsymbol{B}u_{comp} + \boldsymbol{E}i$ (see (12)). Then a suitable compensation signal c as described in (31) is generated and subtracted from the control variable u in order to obtain the new input u_{comp}.

Introducing the observer and compensation into the controlled process as depicted in Figure 3 yields the following disturbed closed loop system:

$$\begin{aligned}\dot{\boldsymbol{x}}_m &= \boldsymbol{A}_m\boldsymbol{x}_m + \boldsymbol{B}_m\left(u_{comp} + \frac{u_{comp}z}{V_0}\right) + \boldsymbol{E}_m i \\ &= \boldsymbol{A}_m\boldsymbol{x}_m + \boldsymbol{B}_m\frac{V_0 + z}{V_0 + \hat{z}}u + \boldsymbol{E}_m i\end{aligned}$$

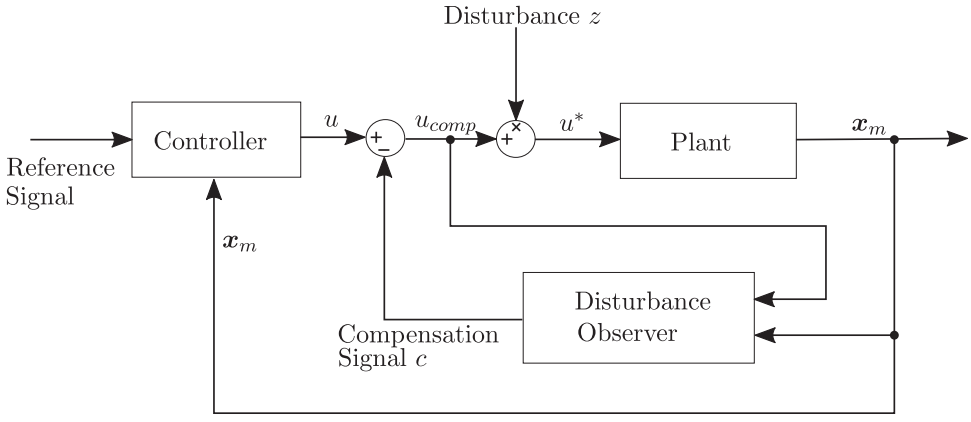

Figure 3. Block diagram of the closed loop system with disturbance compensation.

$$= \boldsymbol{A}_m\boldsymbol{x}_m + \boldsymbol{B}_m u\left(1 + \frac{\tilde{\boldsymbol{C}}\boldsymbol{\varepsilon}}{V_0 + \hat{z}}\right) + \boldsymbol{E}_m i$$

$$= \boldsymbol{A}_m\boldsymbol{x}_m + \boldsymbol{B}_m u + \underbrace{\boldsymbol{B}_m\tilde{\boldsymbol{C}}\frac{1}{V_0 + \hat{z}}\boldsymbol{\varepsilon}}_{=:\boldsymbol{b}} u + \boldsymbol{E}_m i. \tag{34}$$

Because of the additional feedback loop introduced by the compensation, the stability of the observer has to be re-evaluated. In the closed loop system, the input to the observer is given by u_{comp} as it can be seen in Figure 3. The compensated input signal u_{comp} is determined by (31)–(32) and is therefore influenced by the estimated disturbance $\hat{z}$. If $u_{comp} \in [0.49, 820]$, the observer is guaranteed to be stable. If $u_{comp} > 820$, it has to be set to 820: As discussed in Section 2, the input variable u_{comp} is translated into a duty cycle using the formula $d = u_{comp}/820$. So, $u_{comp} > 820$ would lead to a duty cycle larger than one, which is physically impossible, because the emulator's half bridges cannot be closed for more than 100% of the time. If $u_{comp} < 0.49$, the compensation is disconnected and u serves again as the input for the plant and the observer. In a nutshell, every violation of the stability range can be dealt with easily.

Consequently, the expression $\boldsymbol{b}$ in (34) goes to zero exponentially for $\hat{z} \neq -V_0$ (i.e. $\exists k_b, \alpha_b > 0 : \forall t > 0 : ||\boldsymbol{b}(t)||_2^2 \leq k_b \mathrm{e}^{-\alpha_b t}$), because the control variable u is bounded and $\boldsymbol{\varepsilon}$ goes to zero exponentially in the compensated system.

Lastly, apart from the stability of the observer, the stability of the whole system depicted in Figure 3 has to be reviewed. Suppose we have a controller, that stabilises the undisturbed model (2) at an arbitrary but fixed $\boldsymbol{x}^*$. Then it is required that the closed-loop system as described in (34) also stabilises at the same $\boldsymbol{x}^*$. This is indeed the case:

Theorem 3.3 (Closed-Loop Stability): *Let u be such that system (2) converges to a state $\boldsymbol{x}^*$. Then system (34) also converges to $\boldsymbol{x}^*$.*

Proof: The solution of the differential Equation (2), denoted by $\boldsymbol{x}_{m,1}(t)$, is given by

$$\boldsymbol{x}_{m,1}(t) = \mathrm{e}^{\mathbf{A}_m t} + \mathrm{e}^{\mathbf{A}_m t}\int_0^t \mathrm{e}^{-\mathbf{A}_m \tau}\left(\boldsymbol{B}_m u(\tau) + \boldsymbol{E}_m i\right)\,\mathrm{d}\tau. \tag{35}$$

We know that $\lim_{t\to\infty} \boldsymbol{x}_{m,1}(t) = \boldsymbol{x}^*$. For the solution of system (34), denoted by $\boldsymbol{x}_{m,2}(t)$, we obtain

$$\begin{aligned}\boldsymbol{x}_{m,2}(t) &= \mathrm{e}^{\mathbf{A}_m t} + \mathrm{e}^{\mathbf{A}_m t}\int_0^t \mathrm{e}^{-\mathbf{A}_m \tau}\left(\boldsymbol{B}_m u(\tau) + \boldsymbol{E}_m i + \boldsymbol{b}(\tau)\right)\,\mathrm{d}\tau \\ &= \underbrace{\mathrm{e}^{\mathbf{A}_m t} + \mathrm{e}^{\mathbf{A}_m t}\int_0^t \mathrm{e}^{-\mathbf{A}_m \tau}\left(\boldsymbol{B}_m u(\tau) + \boldsymbol{E}_m i\right)\,\mathrm{d}\tau}_{\xrightarrow{t\to\infty}\boldsymbol{x}^*} \\ &\quad + \underbrace{\mathrm{e}^{\mathbf{A}_m t}\int_0^t \mathrm{e}^{-\mathbf{A}_m \tau}\boldsymbol{b}(\tau)\,\mathrm{d}\tau}_{\xrightarrow{t\to\infty}\mathbf{0}}\end{aligned} \tag{36}$$

The second term converges to zero, because $\boldsymbol{b}$ goes to zero exponentially as t goes to infinity and the matrix $\boldsymbol{A}_m$ is Hurwitz. The term $\boldsymbol{b}$ goes to zero exponentially because the observation error does. As a consequence, $\boldsymbol{x}_{m,2}(t)$ also converges to $\boldsymbol{x}^*$. ■

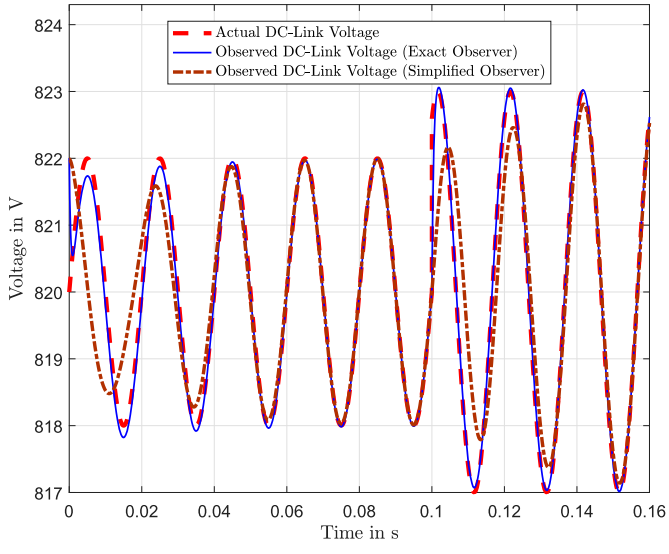

Figure 4. Simulation results: Actual and observed DC-link voltage with a change in the disturbance after 0.1 s. Both observers estimate correctly but the exact observer converges faster.

3.4 Simplified linear version

The observer (12) is exponentially stable for all relevant input trajectories. One drawback, however, is the necessary computing time stemming from the high-dimensional and more or less stiff differential equation system. In this section, we adapt the model and the observer in order to achieve a maximally easy and fast, yet not necessarily stable observer. For that purpose, we define $a_1 := \frac{u\zeta \sin(2\pi ft+\varphi)}{V_0}$ as the new state variable for the disturbance (see (4)). This means that u is seen as a part of the now additive disturbance as we interpret $\frac{u\zeta}{V_0}$ as the amplitude of the disturbance. Consequently, the amplitude is not constant any more, but changes with u. In return, we obtain a completely linear model, which makes observation very easy. However, stability for varying u cannot be guaranteed analytically, because if u changes constantly, the amplitude of the disturbance does as well and therefore there are constantly new errors made in the observation. Furthermore, since only i_1 is directly affected by the input u, it proved sufficient to exclusively use the differential equation for i_1 in the observer in order to further reduce the computational burden. The state equations of the resulting reduced system are given by

$$\begin{pmatrix} \dot{i}_1 \\ \dot{a}_1 \\ \dot{a}_2 \end{pmatrix} = \begin{pmatrix} -\frac{R_1}{L_1} & \frac{1}{L_1} & 0 \\ 0 & 0 & 1 \\ 0 & -\omega^2 & 0 \end{pmatrix} \begin{pmatrix} i_1 \\ a_1 \\ a_2 \end{pmatrix} + \begin{pmatrix} \frac{1}{L_1} \\ 0 \\ 0 \end{pmatrix} u - \begin{pmatrix} \frac{1}{L_1} \\ 0 \\ 0 \end{pmatrix} v_1 \tag{37}$$

with $\omega = 2\pi f$. The measured variable v_1 has to be added as an additional input in order to fulfil the differential equation of i_1. This, of course, introduces a second source of inaccuracy. The measured value v_1 is subject to the disturbance, just like the measured value of i_1. When we use the measured value of

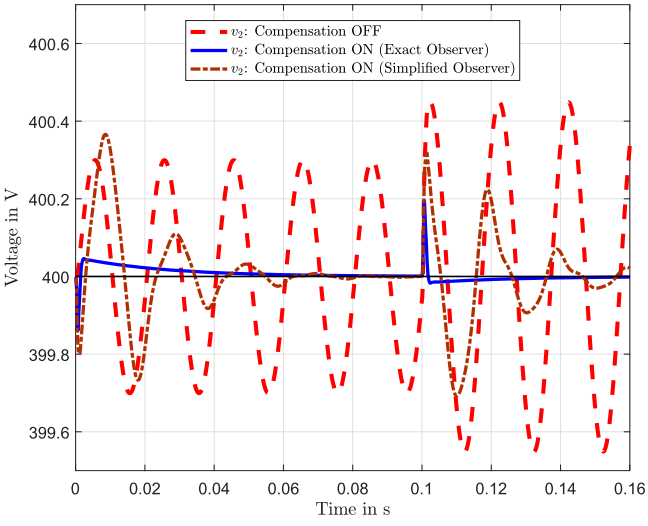

Figure 5. Simulation results: Output voltage with and without compensation. The reference voltage is given by 400 V. The output fluctuations are compensated quickly.

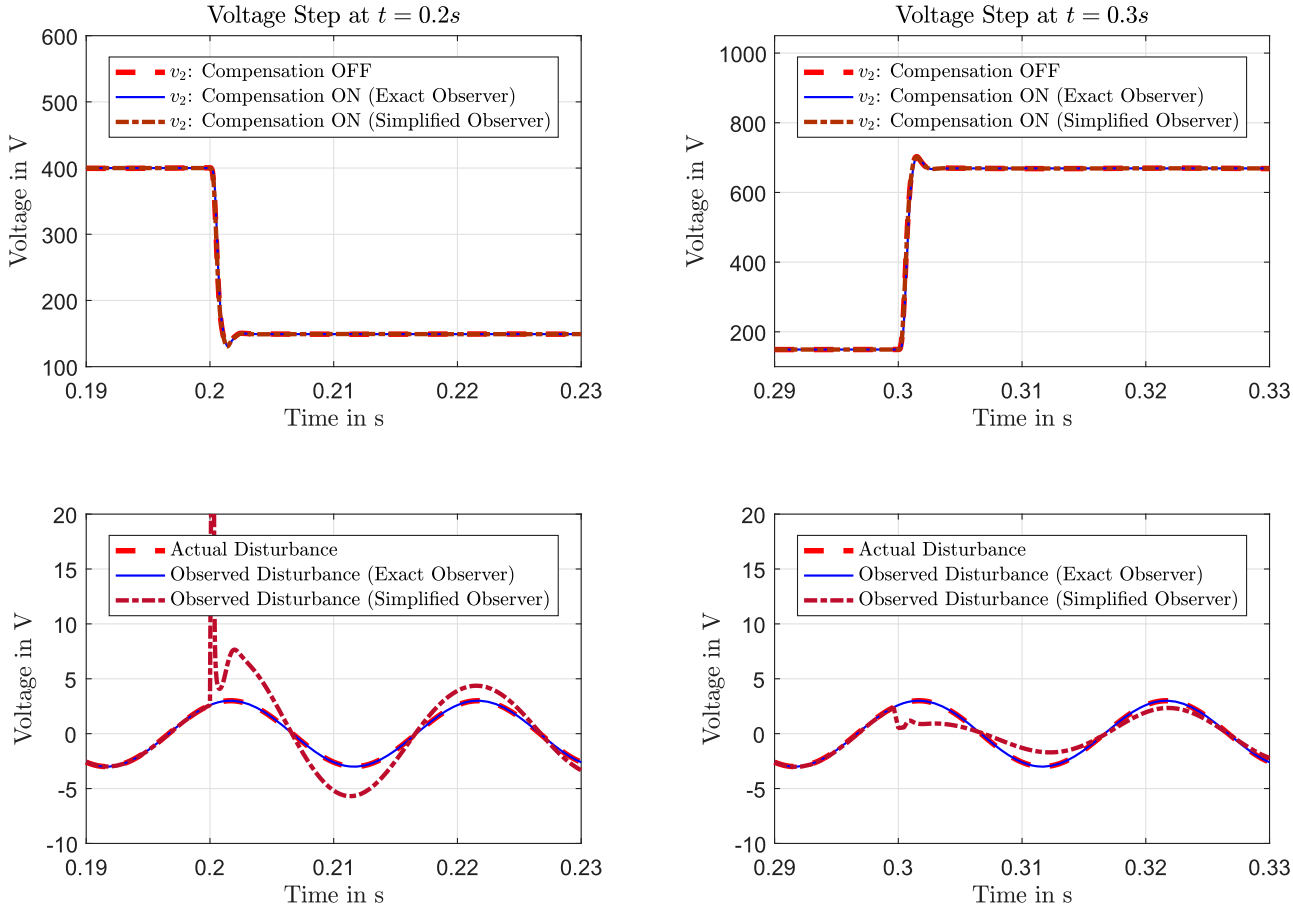

Figure 6. Simulation results: Top panels: The reference voltage changes at $t = 0.2s$ and at $t = 0.3s$. Bottom panels: The exact observer is not influenced by varying reference voltages and matches the true disturbance, whereas the simplified observer produces quite large errors when the reference changes.

v_1 in our observer, the error $i_1 - \hat{i}_1$ cannot be attributed to the disturbance-state a_1 exclusively but also to v_1.

Using Equation (37), a standard linear Kalman filter (see Kalman, 1960) can be used as an observer. The calculation of a suitable compensation signal is not necessary any more and the estimated state $\hat{a}_1$ can be subtracted directly from u. For our problem, the norm of the Kalman gain matrix is several magnitudes smaller than the norm of $\boldsymbol{S}^{-1}$, which shows that the Kalman filter leads to a much less stiff system and is therefore computationally simpler to handle.

4. Results

In this section, we present simulation and experimental results demonstrating the excellent performance of the proposed compensation scheme. All results are based on the parametrisation given in Table 1. All simulation results were obtained through the simulation of the respective continuous models with a simple LQR-controller. In the actual testbed, a model predictive control as described in König et al. (2013) was utilised.

4.1 Simulation results

In the simulation, we assume a constant load current of 100 A and start with a reference output value of 400 V. At first, the disturbance is a sine with a frequency of 50 Hz, an amplitude of 2 V and no phase lag. After 0.1 s of simulation time, the disturbance is altered to an amplitude of 3 V and a phase lag of $\pi/3$ rad. Figure 4 depicts the actual and the DC-link voltage observed by the exact observer (12) and the approximate observer (37). Both observers start with an initial offset of 2 V. The exact observer rapidly adjusts to the actual value. After about 0.02 s there is no difference between actual and observed value visible any longer. Similarly, when the disturbance changes at $t = 0.1$ s, the observer promptly converges towards the new real disturbance. The approximate, linear observer also shows

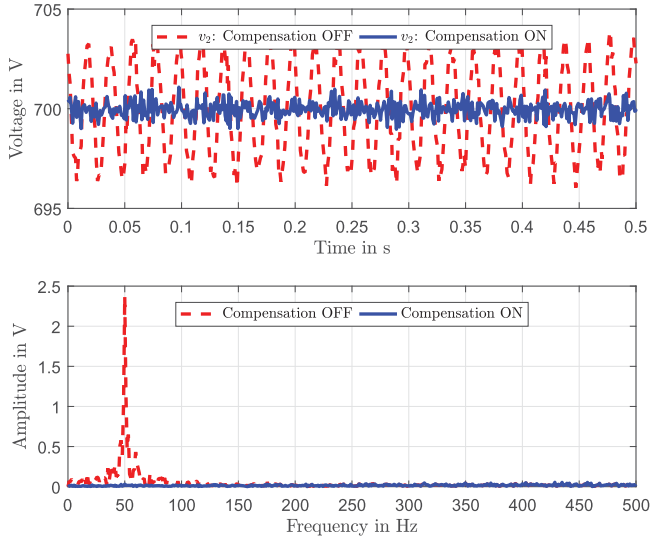

Figure 8. Simulation results: Top panel: Controlled voltage v_2 with and without observation and compensation with simulated measurement noise added. Bottom panel: Spectrum of v_2 with and without observation and compensation. The voltage reference value is given by 700 V and the load current is −190 A.

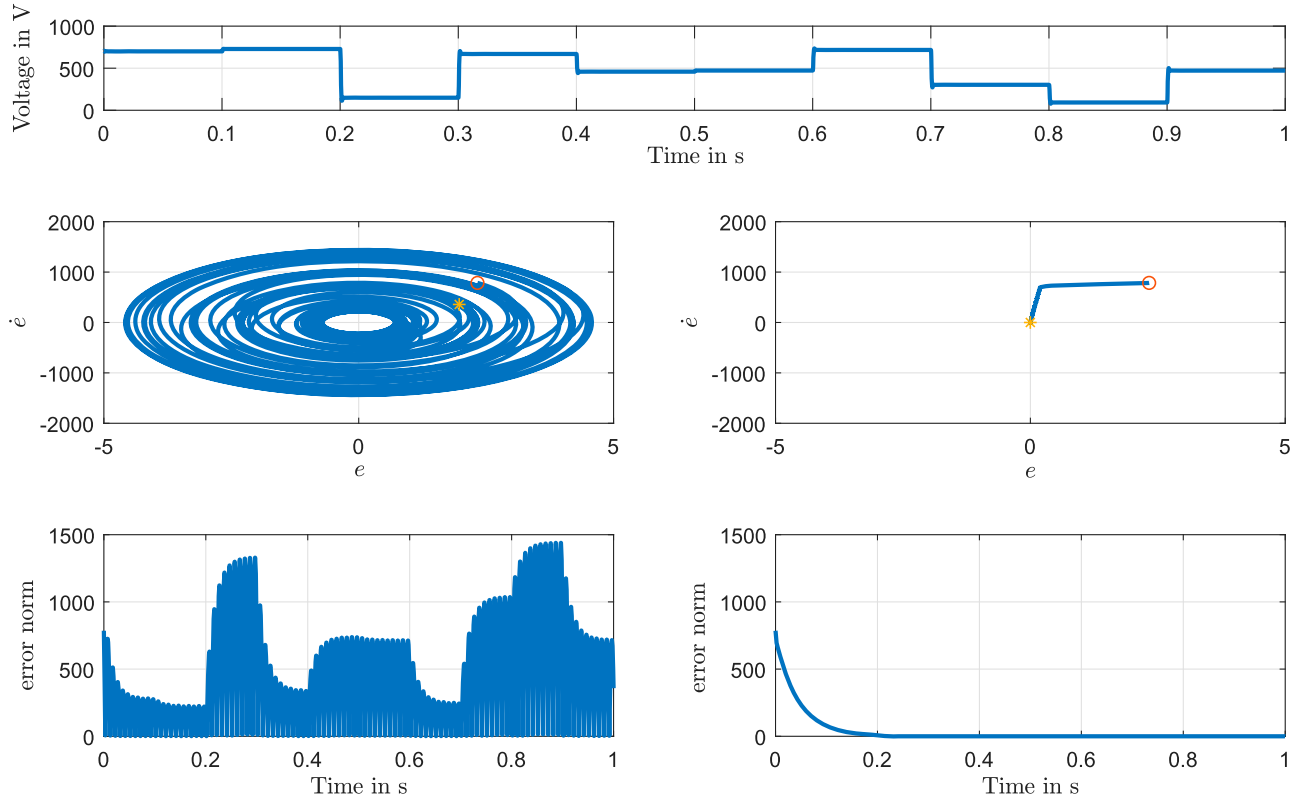

Figure 7. Simulation results: The top panel shows the voltage reference trajectory. The left column depicts a phase portrait and the euclidean norm of the error vector of the simplified observer. The right column illustrates the exact observer.

a satisfying performance. The convergence is slower but still acceptable. When the disturbance changes at $t = 0.1$ s, the linear observer needs noticeably more time to adjust.

Figure 5 illustrates the regulated output voltage v_2 with and without active compensation. The oscillations around the demanded reference value of 400 V are clearly visible in the uncompensated case. With active compensation using the exact observer, however, these oscillations are completely negated and the output voltage matches the reference value. As mentioned before, the observer needs only a minimal amount of time to adjust to the actual disturbance. Once the observation error is eliminated, the output oscillations disappear. When the disturbance is manipulated at $t = 0.1$ s, a small perturbation occurs due to the adjustment of the observer to the new disturbance. The simplified observer cannot eliminate the fluctuations as fast, but given enough time, it can compensate the disturbance as well.

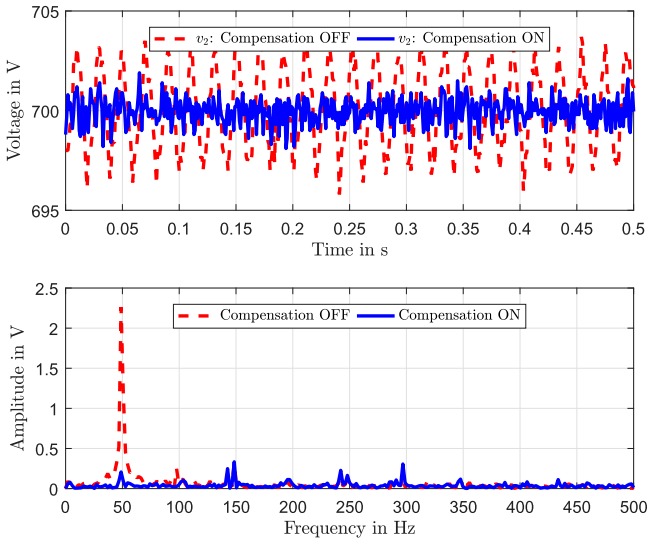

Figure 9. Experimental results: Top panel: Measurements of the controlled voltage v_2 with and without observation and compensation. Bottom panel: Spectrum of v_2 with and without observation and compensation. The experiment was conducted with a voltage target value of 700 V and a load current of −190 A.

In Figure 6, we see how repeated changes in the reference output voltage affect the disturbance estimation. The exact observer is not influenced at all, because the observer explicitly considers the varying inputs. Even though the voltage level influences how strongly the disturbance influences the system (see (4)), the estimation is not affected. In the simplified case, this is very different. As depicted in Figure 6, repeated changes in the reference voltage cause the estimated disturbance to fluctuate heavily. The estimator rarely matches the real disturbance in this case. This is of course not surprising, because the reduced observer ignores the fact that the effect of the disturbance is altered by the input. This performance limitation is the main consequence of reducing the model's complexity. In Figure 7 the evolution of the observer errors of both the exact and simplified observer are analysed in the case of voltage setpoint changes every 0.1 seconds. In the exact case the error and its derivative converge to 0 exponentially. The simplified observer shows no such convergence. Depending on the desired voltage level, the errors increase or decrease. Depending on the variations in the demanded output voltage, the observer errors can therefore increase and stability is not guaranteed if initial observer errors

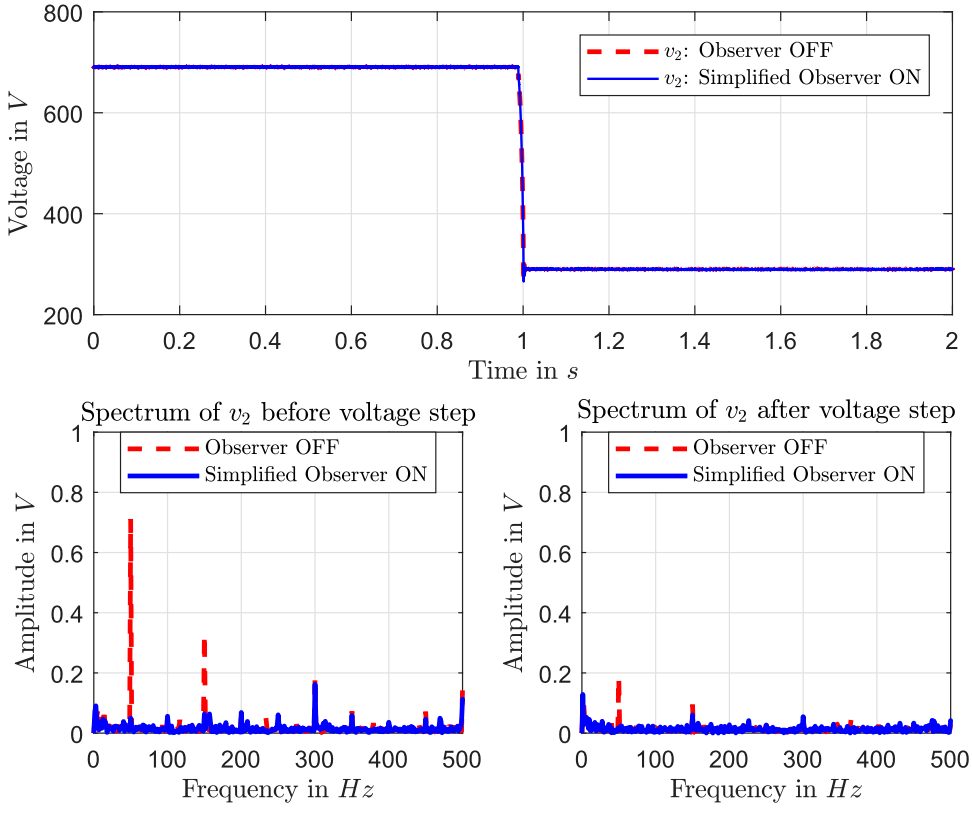

Figure 10. Experimental results with simplified observer: Top panel: Trajectories of the output voltage with and without compensation. Bottom panels: Spectra of the output voltage before and after the setpoint step. The disturbance is compensated by the observer.

accumulate. However, as the simulation depicted in Figure 7 shows, this is not a practical issue, as there is no destabilisation even with such an unrealistic high frequency reference signal. Furthermore, the average execution time is roughly 50% lower for the simplified model which might be a relevant advantage for certain real-time applications. However, the calculation speed of the exact observer can be influenced by choosing different values for $u_{\min}$ or α because these parameters affect the stiffness of the involved differential equations.

4.2 Experimental results

In order to prove the functioning of both observers, we ran various experiments on the battery emulator provided by AVL as described in Section 2.1. First, we compared experimental and simulation results including simulated measurement noise. Figure 8 depicts the simulation and Figure 9 illustrates the experimental results showing measurements and the spectrum of the controlled voltage v_2 with and without observation and compensation using model (37). The results are satisfying. The 50 Hz oscillations are eradicated and only measurement noise remains. In the spectrum, there are no dominant frequencies with active compensation. Furthermore, simulation and experiment look very similar.

Figures 10 and 11 show experiments including a step in the desired output voltage for the simplified and the exact observer, respectively. In both cases the observers are not visibly influenced by the voltage step. Measurement noise and controller-induced undershooting outweigh possible imperfection in the disturbance estimation in the simplified case. It is also clearly visible in the uncompensated spectra, that higher voltage levels are more heavily influenced by the disturbance than lower voltage levels as indicated by (4). In terms of quality of the compensation, there is no significant difference to be found between the two observers. Both versions satisfactorily compensate the leading harmonics.

5. Conclusion

In this paper, we present an observer-based compensation scheme which works independently of the existing control infrastructure. The DC-link fluctuation is modelled using a priori knowledge about its basic structure. This leads to an augmented model where the disturbance is a new state variable. Since the control input is multiplicatively affected by the disturbance, the problem is non-linear. By solving a linear matrix inequality, an exponentially stable observer, inspired by a more complicated state-affine observer, is derived. The estimated disturbance is transformed into a compensation signal that is subtracted from the control input determined by the controller. It is shown that the closed-loop stability of pre-existing controllers is not corrupted by the compensation scheme. Furthermore, a reduced, linear observer is proposed. The simplified observer differential equation is less stiff and is therefore easier to solve for numeric solvers but stability cannot be guaranteed analytically. Finally, simulation and experimental results demonstrate the significant improvements that are achieved by both variants of the compensation.

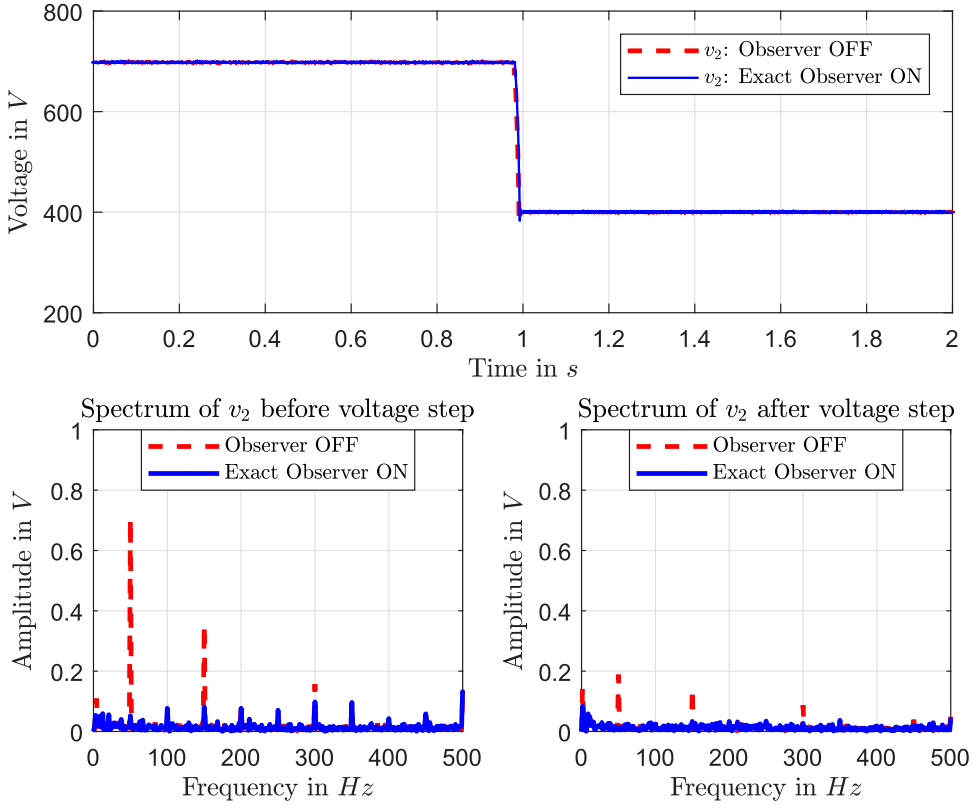

Figure 11. Experimental results with exact observer: Top panel: Trajectories of the output voltage with and without compensation. Bottom panels: Spectra of the output voltage before and after the setpoint step. The disturbance is compensated by the observer. The quality of the compensation scheme is roughly the same as with the simplified observer.

Acknowledgements

The authors acknowledge the TU Wien University Library for financial support through its Open Acces Fundind Program. The financial support by the Christian Doppler Research Association is gratefully acknowledged.

Disclosure statement

No potential conflict of interest was reported by the authors.

References

Adamy, J. (2009). *Nichtlineare regelungen* (1st ed.). Berlin: Springer-Verlag.

Alsmadi, Y. M., Utkin, V., Haj-ahmed, M. A., & Xu, L. (2017). Sliding mode control of power converters: DC/DC converters. *International Journal of Control*, *91*(11), 2472–2493.

Bara, G. I., Daafouz, J., Kratz, F., & Ragot, J. (2001). Parameter-dependent state observer design for affine LPV systems. *International Journal of Control*, *74*(16), 1601–1611.

Besançon, G., León-Morales, J. D., & Huerta-Guevara, O. (2006). On adaptive observers for state affine systems. *International Journal of Control*, *79*(6), 581–591.

Bodson, M. (2001). Performance of an adaptive algorithm for sinusoidal disturbance rejection in high noise. *Automatica*, *37*(7), 1133–1140.

Bodson, M., & Douglas, S. C. (1997). Adaptive algorithms for the rejection of sinusoidal disturbances with unknown frequency. *Automatica*, *33*(12), 2213–2221.

Bodson, M., Sacks, A., & Khosla, P. (1994). Harmonic generation in adaptive feedforward cancellation schemes. *IEEE Transactions on Automatic Control*, *39*(9), 1939–1944.

Bornard, G., Couenne, N., & Celle, F. (1989). Regularly persistent observers for bilinear systems. In J. Descusse, M. Fliess, A. Isidori, & D. Leborgne (Eds.), *New trends in nonlinear control theory. Lecture notes in control and information sciences* (Vol. 122, pp. 130–140). Berlin: Springer.

Chen, W.-H., Yang, J., Guo, L., & Li, S. (2016). Disturbance-Observer-Based control and related methods – An overview. *IEEE Transaction on Industrial Electronics*, *63*(2), 1083–1095.

Chen, X., Li, J., Yang, J., & Li, S. (2013). A disturbance observer enhanced composite cascade control with experimental studies. *International Journal of Control, Automation and Systems*, *11*(3), 555–562.

Ciezki, J., & Ashton, R. (1998). *The application of feedback linearization techniques to the stabilization of DC–DC converters with constant power loads*. Proceedings of the 1998 IEEE International Symposium on Circuits and Systems, ISCAS '98, Monterey, CA (Vol. 3, pp. 526–529).

Corrêa, T. P., König, O., & Greul, R. (2016). *Multisampling in interleaved converters and modular multilevel converters*. IECON 2016-42nd annual conference of the IEEE Industrial Electronics Society, Florence, Italy (pp. 3500–3505). IEEE.

de Jesús Rubio, J., Meléndez, F., & Figueroa, M. (2014). An observer with controller to detect and reject disturbances. *International Journal of Control*, *87*(3), 524–536.

Emadi, A., Khaligh, A., Rivetta, C., & Williamson, G. (2006). Constant power loads and negative impedance instability in automotive systems: Definition, modeling, stability, and control of power electronic converters and motor drives. *IEEE Transactions on Vehicular Technology*, *55*(4), 1112–1125.

Floquet, T., Barbot, J. P., Perruquetti, W., & Djemai, M. (2004). On the robust fault detection via a sliding mode disturbance observer. *International Journal of Control*, *77*(7), 622–629.

Francis, B. A., & Wonham, W. M. (1976). The internal model principle of control theory. *Automatica*, *12*(5), 457–465.

Fuhrmann, M., Euler-Rolle, N., Killian, M., Reinwald, M., & Jakubek, S. (2017). Longitudinal tunnel ventilation control. part 2: Non-linear observation and disturbance rejection. *Control Engineering Practice*, *63*, 44–56.

Gao, Z. (2014). On the centrality of disturbance rejection in automatic control. *ISA Transactions*, *53*(4), 850–857.

Guo, L., & Wen-Hua, C. (2005). Disturbance attenuation and rejection for systems with nonlinearity via DOBC approach. *International Journal of Robust and Nonlinear Control*, *15*(3), 109–125.

Hammouri, H., & de Leon Morales, J. (1990). *Observer synthesis for state-affine systems*. Proceedings of the 29th IEEE Conference on Decision and Control, Honolulu, HI (pp. 784–785).

Jakubek, S., & Jörgl, H. (2000). *Fault-diagnosis and fault-compensation for nonlinear systems*. Proceedings of the 2000 American Control Conference, Chicago, IL (Vol. 5, pp. 3198–3202). IEEE.

Kalman, R. E. (1960). A new approach to linear filtering and prediction problems. *Journal of Basic Engineering*, *82*(1), 35–45.

Khalil, H. K. (2002). *Nonlinear systems* (3rd ed.). Upper Saddle River, NJ: Prentice Hall.

Klein, B., & Olbrot, A. (1986). Observers for state-affine systems. *IEEE Transactions on Automatic Control*, *31*(3), 271–274.

König, O., Gregorčič, G., & Jakubek, S. (2013). Model predictive control of a DC–DC converter for battery emulation. *Control Engineering Practice*, *21*(4), 428–440.

König, O., Hametner, C., Jakubek, S., & Prochart, G. (2015). Datengetriebene Batteriemodelle zur Emulation des Impedanzverhaltens von Traktionsbatterien. *Elektrotechnik and Informationstechnik*, *132*(8), 469–473.

König, O., Hametner, C., Prochart, G., & Jakubek, S. (2013). Battery emulation for power-HIL using local model networks and robust impedance control. *IEEE Transactions on Industrial Electronics*, *61*(2), 428–440.

König, O., Jakubek, S., & Prochart, G. (2011). *Model predictive control of a battery emulator for testing of hybrid and electric powertrains*. 2011 IEEE Vehicle Power and Propulsion Conference, Chicago, IL (pp. 1–6).

Lascu, C., Asiminoaei, L., Boldea, I., & Blaabjerg, F. (2007). High performance current controller for selective harmonic compensation in active power filters. *Ieee Transactions On Power Electronics Pe*, *22*(5), 1826–1835.

Lascu, C., Asiminoaei, L., Boldea, I., & Blaabjerg, F. (2009). Frequency response analysis of current controllers for selective harmonic compensation in active power filters. *IEEE Transactions on Industrial Electronics*, *56*(2), 337–347.

Li, S., Yang, J., Chen, W.-H., & Chen, X. (2014). *Disturbance observer-based control: Methods and applications* (1st ed.). Boca Raton, FL: CRC Press.

Luenberger, D. G. (1964). Observing the state of a linear system. *IEEE Transactions on Military Electronics*, *8*(2), 74–80.

Marino, R., Santosuosso, G. L., & Tomei, P. (2003). Robust adaptive compensation of biased sinusoidal disturbances with unknown frequency. *Automatica*, *39*(10), 1755–1761.

Rahimi, A., & Emadi, A. (2009). Active damping in DC/DC power electronic converters: A novel method to overcome the problems of constant power loads. *IEEE Transactions on Industrial Electronics*, *56*(5), 1428–1439.

Yang, J., Cui, H., Li, S., & Zolotas, A. (2018). Optimized active disturbance rejection control for dc-dc buck converters with uncertainties using a reduced-order gpi observer. *IEEE Transactions on Circuits and Systems I: Regular Papers*, *65*(2), 832–841.

Yang, J., Li, S., Sun, C., & Guo, L. (2013). Nonlinear-disturbance-observer-based robust flight control for airbreathing hypersonic vehicles. *IEEE Transactions on Aerospace and Electronic Systems*, *49*(2), 1263–1275.

Yang, J., Wu, H., Hu, L., & Li, S. (2018). Robust predictive speed regulation of converter-driven DC motors via a discrete-time reduced-order GPIO. *IEEE Transactions on Industrial Electronics, 66*(10), 7893–7903.